

# Carbon Isotopic Abundances in the Red Giants of $\omega$ Centauri (NGC 5139)

Verne V. Smith

*Department of Physics, University of Texas at El Paso, El Paso, TX 79968*

Donald M. Terndrup<sup>1</sup>

*Department of Astronomy, The Ohio State University, Columbus, OH 43210*

and

Nicholas B. Suntzeff

*Cerro Tololo Inter-American Observatory, National Optical Astronomy Observatories, Casilla 603, La Serena, Chile*

## ABSTRACT

Carbon-12 and carbon-13 abundances have been measured in eleven bright giant members of the globular cluster  $\omega$  Centauri via observations of the first-overtone CO bands near  $2.3 \mu\text{m}$ . The stars in this sample were selected to span a substantial fraction of the range of iron abundances found in this cluster. In addition, the sample covers a range of  $[\text{O}/\text{Fe}]$ ,  $[\text{Na}/\text{Fe}]$  and  $[\text{Al}/\text{Fe}]$  abundance ratios derived in previous studies. In all  $\omega$  Cen giants the  $^{12}\text{C}/^{13}\text{C}$  abundance ratio is found to be quite low, indicating deep mixing in these red giants. The mean value for the entire sample is  $\langle ^{12}\text{C}/^{13}\text{C} \rangle = 4.3 \pm 0.4$  ( $\sigma = 1.3$ ), with nine stars equal, within the errors, to the equilibrium ratio  $^{12}\text{C}/^{13}\text{C} = 3.5$  and two stars having slightly higher values. There is no correlation between the  $^{12}\text{C}/^{13}\text{C}$  and the abundance of iron. In addition, no correlation of  $^{12}\text{C}/^{13}\text{C}$  with  $^{12}\text{C}/\text{Fe}$  is found (all giants are deeply mixed), although the derived abundances of  $^{12}\text{C}/\text{Fe}$  show a positive correlation with  $[\text{O}/\text{Fe}]$ , and an anticorrelation with  $[\text{Na}/\text{Fe}]$  (with the oxygen and sodium abundances taken from previous studies in the literature). A comparison of the isotopic carbon ratios in  $\omega$  Cen with those from other globular clusters (M4, M71, NGC6752, and 47 Tuc), and with literature oxygen abundances, may reveal a slight trend of decreasing  $^{12}\text{C}/^{13}\text{C}$  ratios with decreasing  $[\text{O}/\text{Fe}]$  in the entire globular cluster sample of red giants. A comparison between  $^{12}\text{C}/^{13}\text{C}$  and both  $[\text{Na}/\text{Fe}]$  and  $[\text{Al}/\text{Fe}]$ , however, reveals no trend.

*Subject headings:* globular clusters: individual ( $\omega$  Centauri)—nuclear reactions, nucleosynthesis, abundances—stars; abundances—stars: late-type—stars: Population II

---

<sup>1</sup>Visiting Astronomer, Cerro Tololo Inter-American Observatory, National Optical Astronomy Observatories, which are operated by the Association of Universities for Research in Astronomy, Inc., under cooperative agreement with the National Science Foundation.

## 1. Introduction

In the last two decades, it has become clear that evolved giants in metal-poor globular clusters often exhibit a wide range in the abundances of light elements (Paltoglou & Norris 1995; Norris & Da Costa 1995b; Pilachowski, Sneden, & Kraft 1996; Shetrone 1996a, b; Kraft et al. 1997; Sneden et al. 1997; Gonzalez & Wallerstein 1998; Ivans et al. 1999; Smith et al. 2000). These variations are generally agreed to arise from proton capture chains that convert C and O into N, Ne into Na, and Mg to Al in the hydrogen-burning layers of red giants. There has been considerable discussion, however, as to the origin of these abundance patterns (e.g., Cottrell & Da Costa 1981; Kraft 1994; Norris & Da Costa 1995a; Sneden et al. 1997). In the “primordial” scenario, the abundance patterns reflect nucleosynthesis in a prior generation of massive stars; support for this comes from variations in the C, N, O, Na, Mg, and Al abundances among both main-sequence and turn-off stars in various globular clusters, as found by Bell, Hesser, & Cannon (1983), Briley, Hesser, & Bell (1991), Suntzeff & Smith (1991), Briley et al. (1996), Cannon et al. (1998) or Gratton et al. (2001). In contrast, the “evolutionary” scenario envisions that the products of internal proton capture are brought to the stellar surface through mixing in the giants now observed in the clusters. Evidence in favor of this comes from abundance patterns that depend on the evolutionary state of the stars in a cluster. For example, several systems show a decline in the overall carbon abundance with increasing stellar luminosity and a corresponding rise in the abundance of nitrogen, a sharp decline in the ratio of  $^{12}\text{C}/^{13}\text{C}$  from the presumed primordial value near 90 (i.e., the solar value) to values as low as the nuclear equilibrium value of 3.5. This equilibrium ratio of  $^{12}\text{C}/^{13}\text{C} = 3.5$ , which is set largely by the ratio of reaction rates  $^{12}\text{C}(\text{p},\gamma)^{13}\text{N}(\beta^+,\nu)^{13}\text{C}$  and  $^{13}\text{C}(\text{p},\gamma)^{14}\text{N}$ , is insensitive to temperature and is a well-determined astrophysical limit (see the review by Wallerstein et al. 1997). So-called “standard” stellar models evolving up the first ascent of the red giant branch, e.g., Iben (1964) or Charbonnel (1994), predict values to go only as low as  $^{12}\text{C}/^{13}\text{C} \sim 20$ : the differences between the observed (low) isotopic carbon ratios and the higher values predicted by the standard models of stellar evolution has been a longstanding piece of evidence used to invoke extra mixing (or deeper mixing) in red giants. Quite possibly, in the globular cluster stars, both primordial and evolutionary chemical evolution occurs, whereby deep mixing in the current giants is superimposed on preexisting abundance patterns (Briley et al. 1994; Ivans et al. 1999).

Mixing signatures are seen also in metal-poor field giants (Gratton et al. 2000, and references therein), with some interesting differences found between the field stars and globular cluster giants of the same overall metallicity. The O–Na and Mg–Al anticorrelations found in some of the globular clusters are not observed in any of the field red giants. One effect noted in the field giants by Gratton et al. (2000), and also predicted by current non-standard stellar models (Charbonnel 1994; Wasserburg, Boothroyd, & Sackmann 1995; Charbonnel, Brown, & Wallerstein 1998), is that the efficacy of first giant branch mixing will increase as the metallicity decreases. The globular cluster  $\omega$  Centauri is a site where the various mixing trends (as a function of  $[\text{Fe}/\text{H}]$  and as a function of Na and Al variations) can be studied in one object.

The most massive globular in the Milky Way,  $\omega$  Cen has a wide spread of  $[\text{Fe}/\text{H}]^2$  (Suntzeff & Kraft 1996; Norris, Freeman, & Mighell 1996, and references therein), unique among globulars, with the possible exception of M22 (which may show an abundance spread, but much smaller than in  $\omega$  Cen). In  $\omega$  Cen the distribution of  $[\text{Fe}/\text{H}]$  has a floor near  $-2.0$  to  $-1.8$ , presumably representing the initial metallicity of the gas out of which the cluster was formed, and shows an extended tail to higher metal abundances. The abundances of most elements increase with  $[\text{Fe}/\text{H}]$  and exhibit relatively small scatter, with the exception of O, Na, Al and some other light elements (Brown & Wallerstein 1993; Norris & Da Costa 1995b; Smith et al. 2000). As in other globular clusters, the giants of  $\omega$  Cen have  $[\text{Na}/\text{Fe}]$  and  $[\text{Al}/\text{Fe}]$  abundances which are positively correlated with each other, but anticorrelated with  $[\text{O}/\text{Fe}]$  in a way that is most easily (but not definitively!) explained as a product of deep mixing. The abundance patterns of elements heavier than Fe suggest nucleosynthesis from AGB stars between 1 and  $3M_{\odot}$ , but whether this occurred during formation of the cluster that involved self-enrichment, or from mergers of fragments with different chemical abundances, is not yet determined.

To date, only a few measurements of the  $^{12}\text{C}/^{13}\text{C}$  isotopic ratio exist for  $\omega$  Cen giants (3 from Brown & Wallerstein 1993). Their 3 values were all quite low, with  $^{12}\text{C}/^{13}\text{C} = 6, 4$ , and  $4$ ; however, the metallicities sampled by these 3 giants was limited ( $[\text{Fe}/\text{H}] = -1.36, -1.34$ , and  $-1.26$ ). The goal of this work is to derive additional values of  $^{12}\text{C}/^{13}\text{C}$  in a larger sample of  $\omega$  Cen giants, in order to investigate if there are any trends with  $[\text{Fe}/\text{H}]$ , or if this somewhat unique globular cluster differs in its  $^{12}\text{C}/^{13}\text{C}$  ratios when compared to other clusters.

## 2. Observations and Data Reduction

The program stars were selected from the high-resolution study of Norris & Da Costa (1995b), and were chosen to cover a wide range of  $[\text{Fe}/\text{H}]$  at magnitudes where spectroscopy at  $2.35\mu\text{m}$  was practical with a 4m telescope. Most of these stars also have other metallicity determinations from various studies employing low- to high-resolution spectra. Table 1 summarizes the available data for our targets. The first column of that table lists the name of each star from Woolley (1966). The second and third columns list photometry from several sources as assembled by Suntzeff & Kraft (1996); for three stars not tabulated in that paper (ROA 150, 155, and 161), we took the photometry from Cannon & Stobie (1973) and applied a reddening correction of  $E(B - V) = 0.11$  (Butler, Dickens, & Epps 1978). Infrared photometry from Persson et al. (1980) follows in column 4, while the remaining columns show determinations of  $[\text{Fe}/\text{H}]$  from papers listed in the table, all of which are evidently on the same metallicity scale (an exception are the values of Francois, Spite, & Spite (1988), not tabulated here, which are about 0.2 dex lower than in these other studies). We will use the Norris & Da Costa (1995b) values of  $[\text{Fe}/\text{H}]$  throughout the remainder of this paper.

---

<sup>2</sup>Throughout this paper, we will use the normal spectroscopic notation that  $[\text{A}/\text{B}] \equiv \log_{10}(N_{\text{A}}/N_{\text{B}})_{\text{star}} - \log_{10}(N_{\text{A}}/N_{\text{B}})_{\odot}$ , for elements A and B.

In Figure 1 we present a color-magnitude diagram of  $\omega$  Cen. The small points show cluster members ( $\geq 50\%$  membership probability) from van Leeuwen et al. (2000), where the photometry comes from sources referenced in that paper. The large symbols show photometry for our targets. Most of our stars are brighter than the magnitudes where the RGB and AGB are clearly separated, but most should be on the RGB since the evolutionary lifetimes there are much longer than on the AGB.

An additional selection criteria was to observe stars that spanned the range of Na and Al abundances, which in  $\omega$  Cen and other globular clusters are often anticorrelated with oxygen.

Spectra of the first-overtone bands of CO near  $2.3\ \mu\text{m}$  were obtained on June 2–4, 1996, and in a second run on June 10–12, 1998 with the Blanco 4m Telescope and the CTIO infrared spectrometer (DePoy et al. 1990). The 1996 run used an engineering-grade  $256 \times 256$  InSb detector from SBRC which had many defective pixels and an appreciable dark current. The 1998 run employed a similar detector of higher quality, and also was obtained with a tip-tilt secondary. The length of the slit was  $16''$ , and the slit width was set to  $0.7''$ . The pixel size for both runs was  $24\ \mu\text{m}$  for a resolution of  $\lambda/\Delta\lambda \approx 9900\ \text{pixel}^{-1}$ . The effective resolution was obtained from observations of telluric emission lines, which had an average FWHM of 2.7 pixels. A  $K$  filter was used for order separation.

The 1996 observations were obtained in three overlapping wavelength intervals, which are shown in Table 2. In 1998, we obtained spectra at two wavelength settings. These covered the (2–0), (3–1), and (4–2) bands of  $^{12}\text{CO}$  and the (3–1) band of  $^{13}\text{CO}$  and also included features of Ca and Mg (Kleinman & Hall 1986); the latter are, however, very weak in our spectra of the  $\omega$  Cen targets and will not be discussed further. Figure 2 shows two sample calibrated spectra and the identification of the more prominent features. These two giants have similar effective temperatures and metallicities, but note that ROA 155 has noticeably stronger CO bands than ROA 139. Norris & Da Costa (1995b) classify ROA 139 as CN-strong and ROA 155 as CN-weak; the difference between the CN bandstrengths represents differences in the nitrogen abundance (Norris & Da Costa find  $[\text{N}/\text{Fe}] = +1.05$  for ROA 139 and  $+0.40$  for ROA 155). The differing CO bandstrengths observable in Figure 2 fit in with the C–N anticorrelation expected from differing degrees of CN-cycle mixing.

The observing procedure in both years was to obtain repeated spectra with the star placed at various locations along the slit. Exposure times ranged from 30 to 60 seconds at each position, and the motion of the star along the slit between exposures was sufficient to completely separate the spectra on the detector. In both runs, observations of a hot star (HD 116717, spectral type A0V) were interleaved with observations of the  $\omega$  Cen targets. The observing procedure was identical to that used for the program stars, except that since HD 116717 was brighter, the exposure times were shorter and fewer positions along the slit were needed in order to achieve the same, or higher, S/N than in the  $\omega$  Cen stars. Spectra were obtained for several stars at one wavelength interval, then repeated at the other wavelength settings.

Data reduction was performed using scripts written for the IRAF<sup>3</sup> and VISTA packages. The images were first corrected for the nonlinear response of the detectors. The correction multiplied the raw counts by a quadratic polynomial in intensity. The correction was almost always less than 0.5%, but was 2–3% at the center of the spectrum for the brightest stars. Next, the several images for each star were combined via a median, which removed the individual spectra. This was subtracted from the images, thereby correcting for the sky and the dark current. Finally, the images were divided by a flat field, which was obtained by combining many images of a white spot on the telescope dome, obtained in two passes with the dome lights on and off then subtracted.

The resulting spectra were then traced, extracted in an aperture of width twice the FWHM of the spectra, and co-added after multiplicatively scaling to the average mean exposure. The co-adding process computed an average with rejection of pixels that were  $> 4\sigma$  away from the average. The deviation about the mean gave a measure of the S/N per spectrum, which was typically 75 to 120 for the  $\omega$  Cen spectra.

The final step was to correct for the many telluric absorption lines in the spectra using the observations of the spectra of the hot star. When hot star spectra were taken both before and after one of the  $\omega$  Cen targets, we interpolated the spectra linearly in time to the midpoint of the target star’s observation. If spectra were not available that bracketed an observation in  $\omega$  Cen, we always had one adjacent to the observation. We measured the shift in the wavelength direction (in pixels) between the interpolated spectrum and the combined target spectrum to ensure that they were aligned correctly. The resulting pixel shifts were almost always less than 0.3 pixel. Then the object spectrum was divided by the interpolated spectrum.

Because there are few lamp arc lines in the spectral intervals we observed, the wavelength calibration was achieved in several steps. We first computed the linear wavelength solution for the bluest observed wavelength interval in the 1996 spectra, in which there are several OH airglow lines that have wavelengths compiled by Oliva & Origlia (1992). The dispersion ( $\mu\text{m pixel}^{-1}$ ) from this solution was assumed to be the same for the other two wavelength intervals. We determined the zero point for the central wavelength interval by computing the average pixel shift between the two spectrum sections via cross correlation. Finally, the zero point for the red spectral interval was adjusted to match the the 3–1, 2–0 and 4–2 bandheads of  $^{12}\text{CO}$ , where the wavelengths of these were taken from Kleinman & Hall (1986). A similar procedure was followed for the 1998 data, using the airglow lines in the blue spectra to set the dispersion for both wavelength intervals, then adjusting the zero point for the red spectra to match the  $^{12}\text{CO}$  bandheads. The r.m.s. residuals in the solutions using either the telluric lines or the CO bandheads were always less than 0.4 pixels.

---

<sup>3</sup>The IRAF software is distributed by the National Optical Astronomy Observatories under contract with the National Science Foundation

### 3. The Carbon Isotopic Abundance Analysis

An abundance analysis of the carbon isotopes, using the CO features, was carried out for the program stars using the most recent version of the LTE spectrum synthesis code MOOG (Snedden 1973). Model atmospheres were computed using a version of the MARCS code described in Gustafsson et al. (1975), and are plane parallel, hydrostatic equilibrium models. For the  $\omega$  Cen giants spanning the range in temperature, gravity, and metallicity found here, the use of MARCS-type models is appropriate, as discussed in a number of abundance studies, e.g., Smith et al. (2000), Ramirez et al. (2001), or Cunha et al. (2002). In addition, an analysis by Hinkle & Lambert (1975) of the formation of the CO vibration-rotation (V–R) lines in the types of red-giant atmospheres studied here finds that these lines form to a high degree in LTE.

As mentioned in the Introduction, all of the  $\omega$  Cen program stars observed here were analyzed by Norris & Da Costa (1995b), thus detailed abundances from a number of elements are already available. The stellar parameters of effective temperature ( $T_{\text{eff}}$ ), surface gravity ( $\log g$ ), microturbulence ( $\xi$ ), and metallicity (taken as  $[\text{Fe}/\text{H}]$ ) were derived by a combination of photometric and spectroscopic indicators, as discussed by Norris & Da Costa (1995b). A comparison of those parameters, with those derived independently by Smith et al. (2000) for a subset of the Norris & Da Costa (1995b) sample, is described in both Smith et al. (2000) and Cunha et al. (2002). No unexpected systematic errors or uncertainties are found and  $T_{\text{eff}}$ ,  $\log g$ ,  $\xi$ , and  $[\text{Fe}/\text{H}]$ , as derived by Norris & Da Costa (1995b) are adopted here. Estimates of uncertainties in the stellar parameters, as discussed in the various abundance analysis papers mentioned above, are about  $\pm 100\text{K}$  in  $T_{\text{eff}}$ ,  $\pm 0.2$  dex in  $\log g$ ,  $\pm 0.2 \text{ km s}^{-1}$  in  $\xi$ , and  $\pm 0.05$  dex in  $[\text{Fe}/\text{H}]$ . The adopted stellar parameters are shown in the beginning columns of Table 3.

Spectral-line lists covering the regions observed were constructed using the atomic linelist from the Kurucz & Bell (1995) dataset and CO lines from Goorvitch (1994). Lines due to CN in this spectral region were also included and were kindly provided by B. Plez (2001, private communication). For giants with the temperatures and metallicities of our program stars, the CN lines are a minor contribution, even for very large nitrogen enhancements. In all of the program stars the C/O abundance ratio is less than 1.0 and CO formation is controlled primarily by the carbon abundance. Although the derived carbon abundance from CO depends slightly on the oxygen abundance, this dependence is not large for the temperature regime covered here and oxygen abundances are available from Norris & Da Costa (1995b), who used the  $[\text{O I}] \lambda 6300\text{\AA}$  line. With a given O abundance and model atmosphere, the CO bands were synthesized as a function of carbon abundance. Synthetic spectra were calculated with wavelength increments of  $0.01\text{\AA}$  (or  $\lambda/\Delta\lambda = 2.3 \times 10^6$ ) and smoothed with a Gaussian broadening function of  $6.4\text{\AA}$ , corresponding to the measured widths of intrinsically narrow telluric emission lines. Typical internal stellar broadening mechanisms in these giants (thermal, microturbulence, and macroturbulence) are  $\sim 0.8\text{--}1.0\text{\AA}$  at this wavelength, so instrumental broadening is by far the dominant term. The Gaussian smoothing function was found to provide excellent fits to the observed spectra. The  $^{12}\text{C}$  abundance was derived first, giving most weight to the regions covering the  $^{12}\text{CO}$  (3–1) and (4–2) bandheads, as

these are free from  $^{13}\text{CO}$  contamination and were found to be most sensitive to the carbon-12 abundance. A sample comparison and fit between observed and synthetic spectra is shown in Figure 3 for the star ROA155 ( $[\text{Fe}/\text{H}] = -1.64$ ). The top panel shows the  $^{12}\text{CO}$  (3–1) bandhead for three different  $^{12}\text{C}$  abundances. Straightforward least-squares residuals were used to select the best-fit carbon abundance, and this abundance was rounded to the nearest 0.1 dex. Residuals were computed for regions covering  $\sim 23225\text{--}23260\text{\AA}$  for  $^{12}\text{CO}$  (3–1) and  $23515\text{--}23550\text{\AA}$  for  $^{12}\text{CO}$  (4–2). Each region contains about 17 data points, so the minimum sum of squared residuals was not affected significantly by a few deviant points. The bottom panel illustrates the fit for the  $^{13}\text{CO}$  (2–0) bandhead in this star, using the already derived  $^{12}\text{C}$  abundance; the  $^{13}\text{C}$  abundance is parameterized by the  $^{12}\text{C}/^{13}\text{C}$  ratio and synthetic spectra computed for three different isotopic ratios are shown, with  $^{12}\text{C}/^{13}\text{C} = 4.0$  being the best fit. The interval for calculating residuals was  $\sim 23447\text{--}23480\text{\AA}$  containing 16 or 17 data points: the resulting minima were not influenced significantly by the occasional noisy point. Isotopic ratios were rounded to the nearest 0.5.

The primary uncertainties in the derived carbon isotopic abundances arise from uncertainties in the input stellar parameters  $T_{\text{eff}}$ ,  $\log g$ , and microturbulence (the model metallicity has negligible effect on the derived abundances, unless the change in metallicity is substantial, i.e. factors of 10). Tests were done for parameter changes of 100K in effective temperature, 0.2 dex in  $\log g$ , and 0.2  $\text{km s}^{-1}$  in  $\xi$ , with the following results for the change in carbon-12 abundances:  $\Delta T_{\text{eff}} = +100\text{K}$  yields  $\Delta C = +0.05$  dex,  $\Delta(\log g) = +0.2$  dex yields  $\Delta C = +0.05$  dex, and  $\Delta \xi = +0.2 \text{ km s}^{-1}$  yields  $\Delta C = -0.04$  dex. An additional uncertainty arises from the S/N of the spectra, and based on the depth and width of residual minima as a function of carbon abundance, a typical  $1\sigma$  uncertainty is  $\pm 0.04$  dex in  $\Delta C$ . Compared to all of these errors, broadening adds an insignificant uncertainty as the total integrated absorption is conserved and red giants with these temperatures and abundances have flux points close to the continuum blueward of the  $^{12}\text{CO}$  (3–1) bandhead. Adding these abundance errors in quadrature provides an abundance uncertainty of  $\pm 0.09$  dex for carbon. The isotopic ratios are very insensitive to the model parameters, but a conservative estimate based on testing various fits indicates that the ratio itself is uncertain by  $\pm 1.0$  in  $^{12}\text{C}/^{13}\text{C}$ . For all program stars here, Norris & Da Costa (1995b) derived  $^{12}\text{C}$  abundances from the violet CH bands, and a comparison is shown (with both our estimated errors and their estimated errors) in Figure 4. The comparison is quite good, with the mean difference (Us – Norris & Da Costa) being  $+0.14 \pm 0.24$  dex. One star, ROA 139, is the only giant to show a discrepancy (we find  $[\text{C}/\text{Fe}] = -1.13$  while Norris & Da Costa derive  $-0.50$ ). It is worth noting that this star has the most extreme nitrogen abundance found by Norris & Da Costa, with  $[\text{N}/\text{Fe}] = +1.05$ . In a plot of  $[\text{N}/\text{Fe}]$  versus  $[\text{C}/\text{Fe}]$ , assembled from the Norris & Da Costa abundances, ROA 139 stands out as falling well above their mean relation (i.e., quite a large  $[\text{N}/\text{Fe}]$  ratio for their value of  $[\text{C}/\text{Fe}]$ ). Simply extrapolating their  $[\text{N}/\text{Fe}]$ – $[\text{C}/\text{Fe}]$  relation to a large value of  $[\text{N}/\text{Fe}]$  would suggest that ROA 139 should have a very low  $[\text{C}/\text{Fe}]$  ratio ( $\leq -1.0$ ), as we find. It may be that at very low carbon abundances, the violet CH-band becomes quite weak.

The Norris & Da Costa estimated uncertainties of  $\pm 0.21$  dex, coupled with our uncertainties

of  $\pm 0.10$  dex (in  $[\text{C}/\text{Fe}]$ , assuming an uncertainty of 0.05 dex in Fe), yield an expected scatter of 0.23 dex, close to the observed value of 0.24 dex. The small offset of +0.14 dex in the absolute abundance scale probably arises from small differences in the gf-value scales between CH and CO, as well as a possible small difference in the adopted solar carbon abundance. A recent value for the solar carbon abundance is by Holweger (2001), who finds  $\log \epsilon(\text{C}) = 8.59$ . This abundance can be checked from a solar analysis using the same CO lines as those used in our  $\omega$  Cen analysis. We generated a MARCS solar model ( $T_{\text{eff}} = 5777\text{K}$ ,  $\log g = 4.438$ ) with a microturbulent velocity of  $1.0 \text{ km s}^{-1}$  (this value of  $\xi$  yields our preferred iron abundance of  $\log \epsilon(\text{Fe}) = 7.50$ ) from an analysis of both Fe I and Fe II lines with well-defined laboratory oscillator strengths, and is the same solar Fe abundance adopted by Norris & Da Costa (1995b), whose  $\omega$  Cen Fe-abundance scale is used here). The solar flux spectrum used is that from Wallace & Hinkle (1996), which has a spectral resolution of  $\lambda/\Delta\lambda = 261,000$ . Syntheses of the same regions used in the  $\omega$  Cen analysis (23225-23260Å and 23515-23550Å) were examined and the best solar  $^{12}\text{C}$  abundance derived from the  $^{12}\text{CO}$  lines (using a MARCS model) is  $\log \epsilon(\text{C}) = 8.55$ : this is close enough to the Holweger (2001) value that we will adopt 8.59 as the solar  $^{12}\text{C}$  abundance. the two respective solar Fe abundances are the same, with  $\log \epsilon(\text{Fe}) = 7.50$ ). This comparison indicates that the carbon isotopic abundances presented here do not suffer from significant systematic effects. The carbon-12 abundances, as well as the  $^{12}\text{C}/^{13}\text{C}$  ratios are listed in Table 3. The  $[\text{Fe}/\text{H}]$  values from Norris & Da Costa (1995b) are used to also tabulate values of  $^{12}\text{C}/\text{Fe}$ .

#### 4. Results and Discussion

An initial investigation into the isotopic carbon abundance ratios in these  $\omega$  Cen giants is illustrated in Figure 5. In the top panel,  $^{12}\text{C}/^{13}\text{C}$  ratios are plotted as a function of  $[\text{Fe}/\text{H}]$  for various samples of metal-poor giants. A number of globular clusters have been analyzed for isotopic carbon ratios and we include in this discussion the results from Smith & Suntzeff (1989) and Suntzeff & Smith (1991) for M4 (39 giants), Suntzeff & Smith (1991) for NGC6752 (12 giants), Bell, Briley, & Smith (1991) for 47 Tuc (4 giants), and Briley et al. (1997) for M71 (10 giants). In addition, samples of field stars have been analyzed and new results, as well as a summary of earlier work, have been presented most recently by Keller, Pilachowski, & Sneden (2001): these results are also included in the comparisons. Concentrating first on the  $\omega$  Cen giants, there is no significant trend of  $^{12}\text{C}/^{13}\text{C}$  with  $[\text{Fe}/\text{H}]$ , and all member giants show evidence of deep mixing. Two of the more metal-poor  $\omega$  Cen giants have slightly larger ratios (6 for ROA 252 and 7 for ROA 58), however, the overall carbon abundances in these particular stars are quite low and the CO bands weaker. The  $^{13}\text{CO}$  bands in these two giants are weaker than in the other program stars, thus the uncertainties are probably somewhat larger: before a trend could be claimed, a larger sample of  $\omega$  Cen giants would need to be studied. With the current results, no real trend with  $[\text{Fe}/\text{H}]$  is found for the  $\omega$  Cen members.

In general, the  $\omega$  Cen results look very similar to what is found for the other globular clusters,



with the following note: the two fairly metal-rich clusters, M71 and 47 Tuc, appear to have substantial fractions of their members with both slightly high ( $^{12}\text{C}/^{13}\text{C} \sim 7\text{--}8$ ) and low ( $^{12}\text{C}/^{13}\text{C} \sim 4$ ) ratios. Briley et al. (1997) have shown that these ratios are anticorrelated with CN band strengths (the CN-strong giants have lower  $^{12}\text{C}/^{13}\text{C}$  ratios and the CN-weak giants have higher ratios). This dichotomy is not seen in the somewhat more metal-poor clusters M4 and NGC 6752 (although this cluster does have 1 giant in the sample of 12 with a high ratio and it is one of the CN-weak stars). No measurable effect in the C-isotopic ratios as a function of CN strength is found for  $\omega$  Cen:  $^{12}\text{C}/^{13}\text{C} = 4.9 \pm 0.8$  and  $3.5 \pm 0.5$  (m.e.) for the CN-weak and CN-strong stars, respectively: a difference of only  $1.5\sigma$ .

An additional observation that should be noted about the top panel of Figure 5 is that the field-star sample contains a number of quite metal-poor giants with  $^{12}\text{C}/^{13}\text{C}$  ratios of about 8–10, somewhat higher than most of the globular-cluster giants. This point is addressed in the bottom panel of Figure 5, where  $^{12}\text{C}/^{13}\text{C}$  is plotted versus absolute visual magnitude. The field giants with the slightly larger C-isotopic ratios tend to be somewhat less luminous than the globular-cluster sample. The luminosity dependence of  $^{12}\text{C}/^{13}\text{C}$  is discussed by Keller et al. (2001) and the isotopic ratios in the more luminous field giants overlap perfectly with the globular-cluster giants. Again, the  $\omega$  Cen member ROA 58 (with  $^{12}\text{C}/^{13}\text{C} = 7.0$ ) stands out somewhat in this plot; however, as discussed above, this giant has a low carbon abundance and the CO bands are weak: better spectra would need to be obtained, or more  $\omega$  Cen giants observed, in order to decide whether this result for ROA 58 is real or significant. The conclusion from this study is that for these rather luminous  $\omega$  Cen giants, with  $M_V \leq -1.8$ , there is no measurable change in  $^{12}\text{C}/^{13}\text{C}$  versus  $[\text{Fe}/\text{H}]$ .

As discussed in Section 3, the absolute carbon abundances can also be derived fairly accurately for these giants from the CO bands. In Figure 6, a number of isotopic and elemental abundance ratios are plotted versus  $^{12}\text{C}/\text{Fe}$  (hereafter  $[\text{C}/\text{Fe}]$ ): the carbon-12 abundance is predicted to decrease as the envelope fraction of CN-processed material increases. In the mixing scenario a lower  $[\text{C}/\text{Fe}]$  corresponds to deeper mixing, while in the primordial scenario it results from increased pollution from material processed through presumed progenitor stars. The top left panel in Figure 6 shows  $^{12}\text{C}/^{13}\text{C}$  versus  $[\text{C}/\text{Fe}]$  for  $\omega$  Cen and a number of other samples. Concentrating on the  $\omega$  Cen members for the moment, no trend is found, with all  $\omega$  Cen giants having low  $^{12}\text{C}/^{13}\text{C}$  ratios, indicative of envelope material heavily exposed to the CN-cycle, and  $^{12}\text{C}$  to Fe ratios spanning about a factor of 10. Correlations between  $^{12}\text{C}$ , O, and Na are explored in the bottom left and top right panels of Figure 6. In these panels there is clear correlation between  $[\text{O}/\text{Fe}]$  versus  $[\text{C}/\text{Fe}]$  and an anti-correlation between  $[\text{Na}/\text{Fe}]$  versus  $[\text{C}/\text{Fe}]$  (the Na and O abundances for  $\omega$  Cen are from Norris & Da Costa 1995b). As discussed in the Introduction, these are the trends expected for material exposed to H-burning. Anticorrelations between  $[\text{Na}/\text{Fe}]$  and  $[\text{O}/\text{Fe}]$ , are found in many globular clusters, e.g., Langer, Hoffman, & Sneden (1993), Kraft et al. (1993), Pilachowski et al. (1996), or Kraft et al. (1998). One interpretation of these Na–O anticorrelations is deep mixing in the currently observed giants, although Briley et al (1996) find Na–CN anticorrelations in 47 Tuc turnoff stars, while Cannon et al. (1998) find C–N anticorrelations in 47 Tuc main-sequence

stars, and Gratton et al. (2001) have found Na–O anticorrelations in main-sequence members of NGC6752. The ultimate origins of these various abundance correlations and anticorrelations observed in a number of globular clusters are still not understood completely.

Other globular clusters are plotted in Figure 6 as comparisons to  $\omega$  Cen. In the top left panel, results are available for five other clusters, as well as field stars. Omega Cen does not obviously stand out relative to the other globular clusters. In the bottom left panel of Figure 6 results for the clusters M4 and M71 are compared to those from  $\omega$  Cen; the [O/Fe] values for M4 are from Ivans et al. (1999) and for M71 from Briley et al. (1997). Oxygen abundances are not available for the samples we are using as comparisons for NGC6752 and 47 Tuc. All three globular clusters plotted show a large degree of overlap in the trend of oxygen versus carbon; however,  $\omega$  Cen displays a larger range in values of both [C/Fe] and [O/Fe]. Along a similar line, the top right panel of Figure 6 shows [Na/Fe] versus [C/Fe] for the  $\omega$  Cen stars, along with the M4 sample (with the [Na/Fe] coming from Ivans et al. 1999). An anticorrelation of Na and C is found in both clusters and the trends are, within the uncertainties, identical. Again, though,  $\omega$  Cen displays a larger range in values of [Na/Fe] relative to M4. Greater differences in [C/Fe], [O/Fe], and [Na/Fe] could indicate either deeper mixing (in the mixing scenario) or, on the other hand, larger amounts of pollution from material processed through H-burning (in the primordial scenario). In a recent study of M71, Ramirez & Cohen (2002) have summarized [Na/Fe] and [O/Fe] trends for 11 globular clusters (their Figure 12) and these different clusters display a range in their respective values of both [Na/Fe] and [O/Fe]. If this range is quantified simply as the difference between the largest and smallest values, a weak trend is found between a larger range in [Na/Fe] and [O/Fe] with decreasing [Fe/H]. It is not clear how  $\omega$  Cen fits into this possible trend, as these other clusters have no spread in [Fe/H], whereas the spread in  $\omega$  Cen exceeds a factor of 20; however the range in O and Na to Fe ratios displayed by  $\omega$  Cen members is as large as any found in the other globular clusters, with M13 and M92 showing the largest ranges.

A somewhat different type of chemical behavior is probed in the bottom-right panel of Figure 6, where a slow neutron-capture (s-process) element (La) is plotted versus [C/Fe] for both  $\omega$  Cen and M4. Omega Cen is peculiar in that its member stars display a large increase, in proportion to Fe, of s-process elements as [Fe/H] increases: such behavior is not observed in any other stellar population. The increase in s-process abundances originates from thermally-pulsing asymptotic giant branch (TP-AGB) stars, and the cause of their apparently large contribution to the chemical evolution in  $\omega$  Cen (Lloyd Evans 1983) remains a mystery, although speculation as to the reason can be found in Smith et al. (2000) and Cunha et al. (2002). In this panel no trend is found between [La/Fe] and [C/Fe], indicating that the sources of La enrichment and C depletion are not related. The more La-poor giants in  $\omega$  Cen again overlap perfectly with their counterparts in M4.

Possible correlations of  $^{12}\text{C}/^{13}\text{C}$  with abundances of three elements either destroyed (O) or produced (Na and Al) by various proton capture cycles are explored in Figure 7. The top panel plots the isotopic carbon ratios versus [O/Fe] for  $\omega$  Cen, M4, and M71. In the regions of overlap between these three globular clusters, there is excellent agreement between  $^{12}\text{C}/^{13}\text{C}$  ratios and

[O/Fe] abundance ratios. When taken together, the three cluster samples hint of a correlation between  $^{12}\text{C}/^{13}\text{C}$  and [O/Fe]. This possible trend needs to be verified by future studies of larger samples, but it may point towards a deep-mixing signature in the current globular cluster giants. The bottom two panels, with  $^{12}\text{C}/^{13}\text{C}$  versus [Na/Fe] and [Al/Fe] show no hint of any trend. This is somewhat puzzling in light of the possible trend of the carbon isotopic ratio with [O/Fe]. The deeper and more extensive mixing necessary to enhance the [Na/Fe] and [Al/Fe] ratios, would be expected to drive the envelope C-isotope ratios to their CN-equilibrium value of 3.5: this is not observed. The lack of any correlation between  $^{12}\text{C}/^{13}\text{C}$  and Na or Al points to the origins of some of these abundance variations as arising in some other site, and not in the current cluster giants, as concluded earlier by Briley et al. (1997). A larger sample of  $^{12}\text{C}$ ,  $^{13}\text{C}$ , O, Na, and Al abundances from globular cluster giants would be able to shed more light on this issue.

## 5. Conclusions

The  $^{12}\text{C}/^{13}\text{C}$  ratios in all of the  $\omega$  Cen giants are quite low, with a mean  $\langle^{12}\text{C}/^{13}\text{C}\rangle = 4.3 \pm 0.4$ : this indicates extensive and deep mixing in these low-mass, low-metallicity giants. This result is in general agreement with previous studies of globular cluster giants, as well as low-metallicity field giants. In particular for the  $\omega$  Cen giants, all of which have  $M_V \leq -1.8$ , there is no measurable change in  $^{12}\text{C}/^{13}\text{C}$  over the metallicity range of [Fe/H] = -1.7 to -0.7. It is found that  $[^{12}\text{C}/\text{Fe}]$  correlates well with [O/Fe] and anticorrelates with [Na/Fe], and that the overall trends among these various ratios agrees very well between  $\omega$  Cen and other globular clusters. The  $^{12}\text{C}/^{13}\text{C}$  ratios themselves exhibit no measurable trends with [Na/Fe] or [Al/Fe], but may hint at a positive correlation with [O/Fe].

We wish to thank the staff of the Cerro Tololo Inter-American Observatory, especially M. Fernández and H. Tirado, for their excellent assistance with the observations. Partial support for this project came from the National Science Foundation under grants AST-9157038 and INT-9215844 to The Ohio State University Research Foundation. VVS acknowledges support from the National Science Foundation through grant AST-9987374.

## REFERENCES

- Bell, R. A., Briley, M. M., and Smith, G. H. 1990, *AJ*, 100, 187
- Bell, R. A., Hesser, J. E., & Cannon, R. D. 1983, *ApJ*, 269, 580
- Briley, M. M., Hesser, J. E., & Bell, R. A. 1991, *ApJ*, 373, 482
- Briley, M. M., Bell, R. A., Hesser, J. E., & Smith, G. H. 1994, *Canadian J. Phys.* 72, 772

- Briley, M. M., Smith, V. V., Suntzeff, N. B., Lambert, D. L., Bell, R. A., & Hesser, J. E. 1996, *Nature*, 383, 604
- Briley, M. M., Smith, V. V., King, J., & Lambert, D. L. 1997, *AJ*, 113, 306
- Brown, J. A., & Wallerstein, G. 1993, *AJ*, 106, 133
- Butler, D., Dickens, R. J., & Epps, E. 1978, *ApJ*, 225, 148
- Cannon, R. D., & Stobie, R. S. 1973, *MNRAS*, 162, 207
- Cannon, R. D., Croke, B. F. W., Bell, R. A., Hesser, J. E., & Stathakis, R. A. 1998, *MNRAS*, 298, 601
- Charbonnel, C. 1994, *A&A*, 282, 811
- Charbonnel, C., Brown, J. A., & Wallerstein, G. 1998, *A&A*, 332, 204
- Cottrell, P. L., & Da Costa, G. S. 1981, *ApJ*, 245, L79
- Cunha, K., Smith, V. V., Suntzeff, N. B., Norris, J. E., Da Costa, G. S., & Plez, B. 2002, *AJ*, submitted
- DePoy, D. L., Gregory, B., Elias, J., Montané, A., Pérez, G., & Smith, R. M. 1990, *PASP*, 102, 1433
- Francois, P., Spite, M., & Spite, F. *A&A*, 191, 267
- Gonzalez, G., & Wallerstein, G. 1998, *AJ*, 116, 765
- Goorvitch, D. 1994, *ApJS*, 92, 311
- Gratton, R. G., Sneden, C., Carretta, E., & Bragaglia, A. 2000, *A&A*, 354, 169
- Gratton, R. G., Bonifacio, P., Bragaglia, A., Carretta, E., Castellani, V., Centurion, M., Chieffi, A., Claudi, R., Clementini, G., D’Antona, F., Desidera, S., Francois, P., Grundahl, F., Lucatello, S., Molaro, P., Pasquini, L., Sneden, C., Spite, F., Straniero, O. 2001, *Å*, 369, 87
- Gustafsson, B. E., Bell, R. A., Eriksson, K., & Nordlund, A. 1975, *Å*, 42, 407
- Hinkle, K. H., & Lambert, D. L. 1975, *MNRAS*, 170, 447
- Holweger, H. 2001, in *Solar and Galactic Composition*, ed. R. F. Wimmer-Schweingruber (American Institute of Physics: New York), p.23
- Iben, Jr., I. 1964, *ApJ*, 140, 1631
- Ivans, I. I., Sneden, C., Kraft, R. P., Suntzeff, N. B., Smith, V. V., Langer, G. E., & Fulbright, J. P. 1999, *AJ*, 118, 1273

- Keller, L. D., Pilachowski, C. A., & Sneden, C. 2001, *AJ*, 122, 2554
- Kleinmann, S. G., & Hall, D. N. B. 1986, *ApJS*, 62, 501
- Kraft, R. P., Sneden, C., Langer, G. E., & Shetrone, M. D. 1993, *AJ*, 106, 1490
- Kraft, R. P. 1994, *PASP*, 106, 553
- Kraft, R. P., Sneden, C., Smith, G. G., Shetrone, M. D., Langer, G. E., & Pilachowski, C. A. 1997, *AJ*, 113, 279
- Kraft, R. P., Sneden, C., Smith, G. H., Shetrone, M. D., & Fulbright, J. 1998, *AJ*, 115, 1500
- Kurucz, R. L., & Bell, B. 1995, CD-ROM 23 (Cambridge: SAO)
- Langer, G. E., Hoffman, R., & Sneden, C. 1993, *PASP*, 105, 301
- Lloyd Evans, T. 1983, *MNRAS*, 204, 975
- Norris, J. E., & Da Costa, G. S. 1995a, *ApJ*, 441, L81
- Norris, J. E., & Da Costa, G. S. 1995b, *ApJ*, 447, 680
- Norris, J. E., Freeman, K. C., & Mighell, K. J. 1996, *ApJ*, 462, 241
- Oliva, E., & Origlia, L. 1992, *A&A*, 254, 466
- Paltoglou, G., & Norris, J. E., 1989, *ApJ*, 336, 185
- Persson, S. E., Cohen, J. G., Matthews, K., Frogel, J. A., & Aaronson, M. 1980, *ApJ*, 235, 452
- Pilachowski, C. A., Sneden, C., & Kraft, R. P. 1996, *AJ*, 111, 1689
- Ramirez, S. V., Sellgren, K., Carr, J. S., Balachandran, S. C., Blum, R., Terndrup, D. M., & Steed, A. 2000, *ApJ*, 537, 205
- Ramirez, S. V., & Cohen, J. G. 2002, *AJ*, 123, 3277
- Shetrone, M. D. 1996a, *AJ*, 112, 1517
- Shetrone, M. D. 1996b, *AJ*, 112, 2639
- Smith, V. V., Suntzeff, N. B., Cunha, K., Gallino, R., Busso, M., Lambert, D. L., & Straniero, O. 2000, *AJ*, 119, 1239
- Sneden, C. 1973, Ph.D. thesis, Univ. Texas
- Sneden, C., Kraft, R. P., Shetrone, M. D., Smith, G. H., Langer, G. E., & Prosser, C. F. 1997, *AJ*, 114, 1964

- Suntzeff, N. B., & Kraft, R. P. 1996, *AJ*, 111, 1913
- Suntzeff, N. B., & Smith, V. V. 1991, *ApJ*, 381, 160
- van Leeuwen, F., Le Poole, R. S., Reijns, R. A., Freeman, K. C., & de Zeeuw, P. T. 2000, *A&A*, 360, 472
- Wallerstein, G., Iben, Jr., I., Parker, P., Boesgaard, A. M., Hale, G. M., Champagne, A. E., Barnes, C. A., Käppeler, F., Smith, V. V., Hoffman, R. D., Timmes, F. X., Sneden, C., Boyd, R. N., Meyer, B. S., Lambert, D. L. 1997, *Rev.Mod.Phys.*, 69, 995
- Wasserburg, G. J., Boothroyd, A. I., & Sackmann, I.-J. 1995, *ApJ*, 447, L37
- Woolley, R. v.d.R. 1966, *R. Obs. Ann.*, No. 2

Fig. 1.— Color-magnitude diagram for proper motion members of omega Cen from van Leeuwen et al. (2000), shown as small symbols. The photometry for the stars in the current sample are shown as large points.

Fig. 2.— Sample spectra of two  $\omega$  Cen giants. Both of these giants have similar effective temperatures and metallicities ( $[\text{Fe}/\text{H}]$ ). The prominent  $^{12}\text{CO}$  and  $^{13}\text{CO}$  bands are identified and most of the structure observed as a function of wavelength is real (being composed of many CO vibration-rotation lines). The spectra are normalized and shifted in relative flux so both can be viewed clearly. Note that ROA 139 has weaker CO bands than ROA 155, indicating a lower total carbon abundance in ROA 139, although both have quite low isotopic ratios ( $^{12}\text{C}/^{13}\text{C}=4.5$  for ROA 155 and 3.5 for ROA 139).

Fig. 3.— Observed (solid dots) and synthetic (continuous curves) spectra for the  $\omega$  Cen giant ROA155 ( $T_{\text{eff}} = 4200\text{K}$ ,  $\log g = 0.8$ ,  $\xi = 2.0 \text{ km s}^{-1}$ , and  $[\text{Fe}/\text{H}] = -1.64$ ). The top panel shows a region near the  $^{12}\text{CO}$  (3-1) bandhead, with synthetic spectra calculated for three different  $^{12}\text{C}$  abundances (the best-fit abundance and  $\pm 0.1$  dex). The abundance notation  $A(x) = \log \epsilon(x) = \log(N_x/N_H + 12.0)$  is used. The bottom panel shows the  $^{13}\text{CO}$  (2-0) bandhead region with three synthetic spectra computed with three different isotopic carbon abundance ratios.

Fig. 4.— A comparison of carbon-12 abundances (plotted as  $^{12}\text{C}/\text{Fe}$ ) derived here using CO and derived by Norris & Da Costa (1995b) using violet CH. The solid line illustrates perfect agreement. Errorbars are taken from the discussions in Norris & Da Costa and here. The agreement between the two studies is good, with a mean difference of  $(\text{This Study} - \text{Norris \& Da Costa}) = +0.14 \pm 0.24$  dex: the scatter is that expected given the respective errors in each study.

Fig. 5.— Isotopic carbon abundance ratios are plotted as a function of  $[\text{Fe}/\text{H}]$  (top panel) and absolute visual magnitude (bottom panel) for the different samples of metal-poor giants. There are no strong trends with metallicity, although it should be noted that the scatter in  $^{12}\text{C}/^{13}\text{C}$  in the more metal-rich globular clusters M71 and 47 Tuc is anticorrelated with the CN strengths (Briley et al. 1997). The field sample also contains a number of giants with somewhat higher isotopic ratios ( $\sim 9$ – $10$ ) at lower metallicities; however, the bottom panel reveals these field giants to be of somewhat lower luminosities than most of the globular cluster giants analyzed. The bottom panel reveals a modest trend of decreasing  $^{12}\text{C}/^{13}\text{C}$  as the giant’s luminosity increases (as discussed by Keller et al. 2001): the globular cluster giants fall on the same trend defined by the field-giant population.

Fig. 6.— Comparisons of four different abundance ratios versus  $^{12}\text{C}/\text{Fe}$ . The top left panel shows  $^{12}\text{C}/^{13}\text{C}$  versus  $^{12}\text{C}/\text{Fe}$  for  $\omega$  Cen and a number of different samples of low-metallicity giants. No strong trends are evident, with all giants mixed extensively. The bottom left panel shows correlations between  $[\text{O}/\text{Fe}]$  and  $^{12}\text{C}/\text{Fe}$  in three globular clusters:  $\omega$  Cen, M4, and M71. The respective trends for all three clusters overlap and the correlation of depleted carbon-12 with oxygen is a signature of material processed through the CNO cycles. The top left panel illustrates

the anticorrelation between  $[\text{Na}/\text{Fe}]$  and  $^{12}\text{C}/\text{Fe}]$  in  $\omega$  Cen and M4, again with substantial overlap in the two clusters. The decrease in carbon-12 is due to mixing, while the increase in sodium is due, presumably, to the Na–Ne cycle. The bottom right panel explores the relation between lanthanum, an s-process element, and  $^{12}\text{C}$  in  $\omega$  Cen and M4. No trends exist, indicating that the mixing responsible for  $^{12}\text{C}$  depletion has no dependence on the s-process production site.

Fig. 7.— An investigation of possible trends of  $^{12}\text{C}/^{13}\text{C}$  with O, Na, and Al. In the top panel isotopic carbon ratios are plotted versus  $[\text{O}/\text{Fe}]$  for  $\omega$  Cen, M4, and M71. The three globular clusters together indicate a possible systematic decrease, towards the CN-equilibrium value, in  $^{12}\text{C}/^{13}\text{C}$  as  $[\text{O}/\text{Fe}]$  decreases: this might signify deep mixing in the observed giants. The middle and bottom panels show  $^{12}\text{C}/^{13}\text{C}$  versus  $[\text{Na}/\text{Fe}]$  and  $[\text{Al}/\text{Fe}]$ , respectively, with no measurable trends between these abundance ratios.



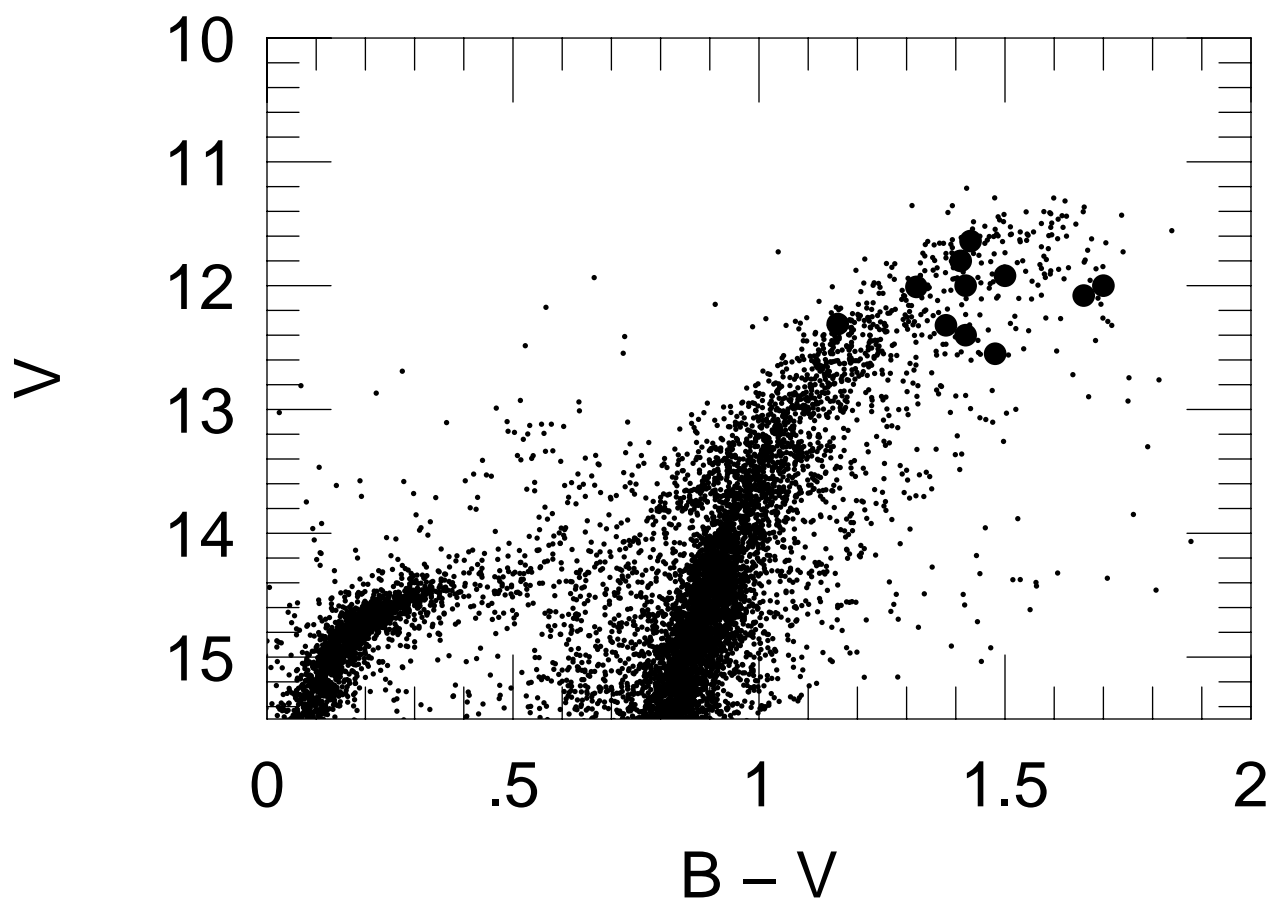


Table 1. Program Star Photometry and Metallicities

Star (ROA)	$V$	$(B - V)_0$	$(V - K)_0$	$[\text{Fe}/\text{H}]^{\text{a}}$	$[\text{Fe}/\text{H}]^{\text{b}}$	$[\text{Fe}/\text{H}]^{\text{c}}$	$[\text{Fe}/\text{H}]^{\text{d}}$
58	11.64	1.33	3.14	−1.77	−1.73	...	−1.72 <sup>e</sup>
91	11.80	1.30	3.14	−1.73	−1.73	...	...
139	11.92	1.39	3.17	−1.57	−1.46	...	...
150	12.00	1.59	3.53	...	−1.25	...	−1.28 <sup>e</sup>
155	12.00	1.31	3.11	...	−1.64	...	...
161	12.01	1.32	3.03	...	−1.67	...	−1.66 <sup>e</sup>
162	12.08	1.55	3.52	−1.26	−1.10	...	...
252	12.31	1.05	...	−1.76	−1.74	...	...
253	12.23	1.27	2.93	−1.38	−1.39	−1.43	...
287	12.40	1.31	3.01	−1.35	−1.43	...	−1.36 <sup>f</sup>
357	12.55	1.10	3.47	−0.85	−0.85	...	...

<sup>a</sup>Suntzeff & Kraft (1996).

<sup>b</sup>Norris & Da Costa (1995).

<sup>c</sup>Smith et al. (2000).

<sup>d</sup>Other determinations of  $[\text{Fe}/\text{H}]$  as follows:

<sup>e</sup>Paltoglou & Norris (1989).

<sup>f</sup>Brown & Wallerstein (1993).

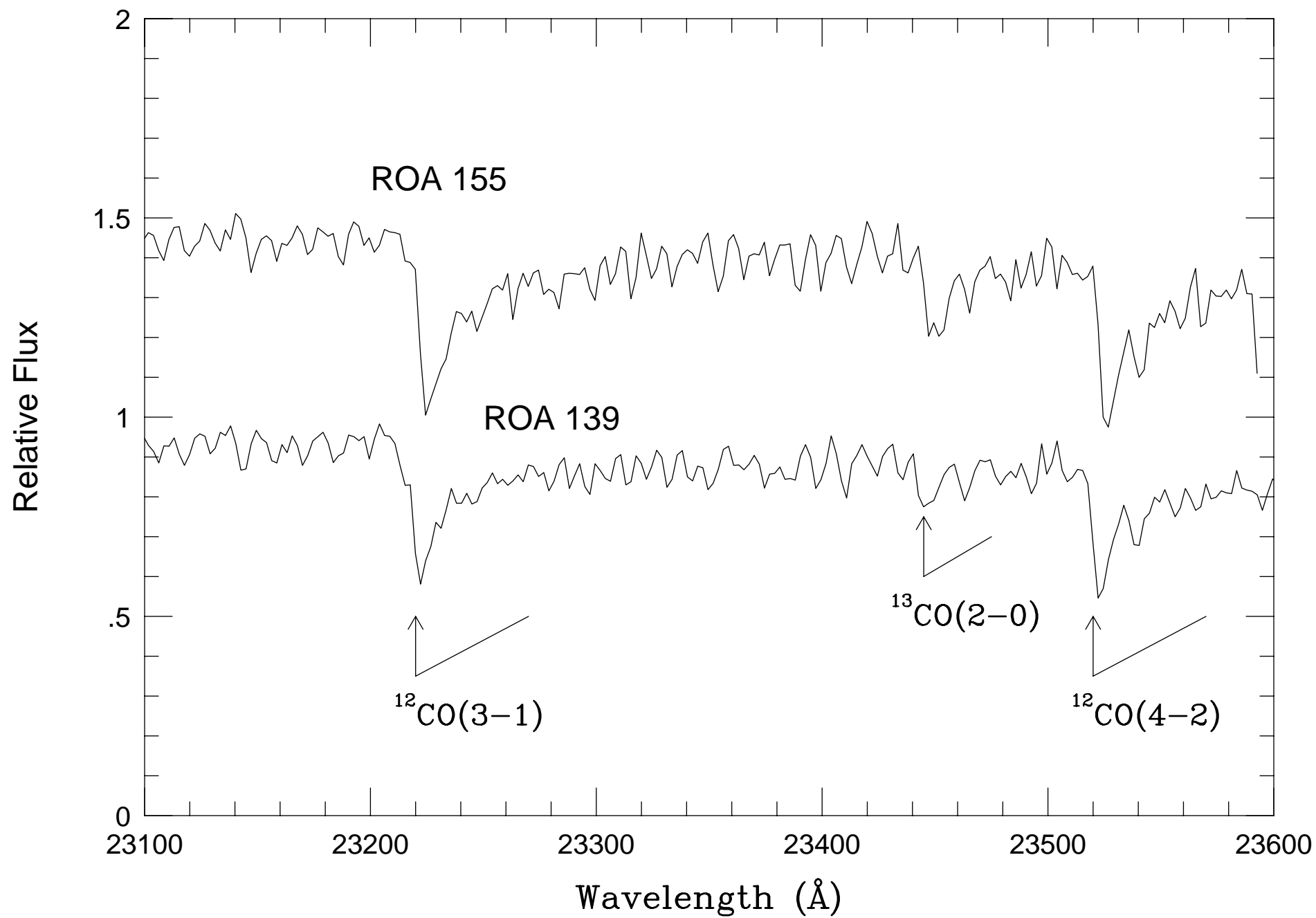


Table 2. Observed wavelength intervals ( $\mu\text{m}$ )

Spectrum	$\lambda(\text{min})$	$\lambda(\text{max})$	$\Delta\lambda^{\text{a}}$
1996 data			
blue	2.2069	2.2789	$2.27289 \times 10^{-4}$
central	2.2529	2.3109	$\dots$
red	2.3033	2.3613	$\dots$
1998 data			
blue	2.2560	2.3172	$2.25084 \times 10^{-4}$
red	2.3085	2.3664	$\dots$

<sup>a</sup>Derived for this spectrum interval and assumed to apply to the others.

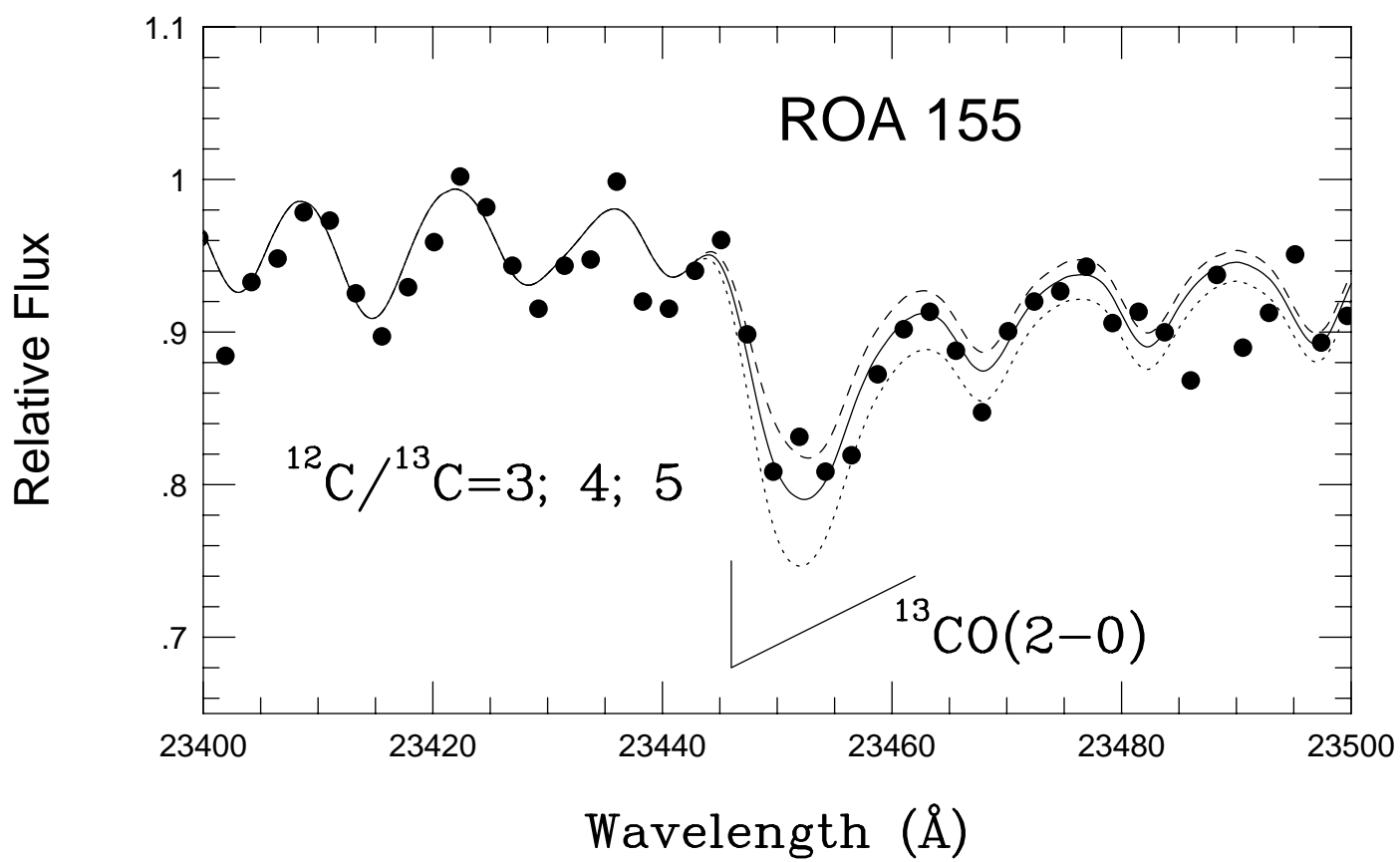
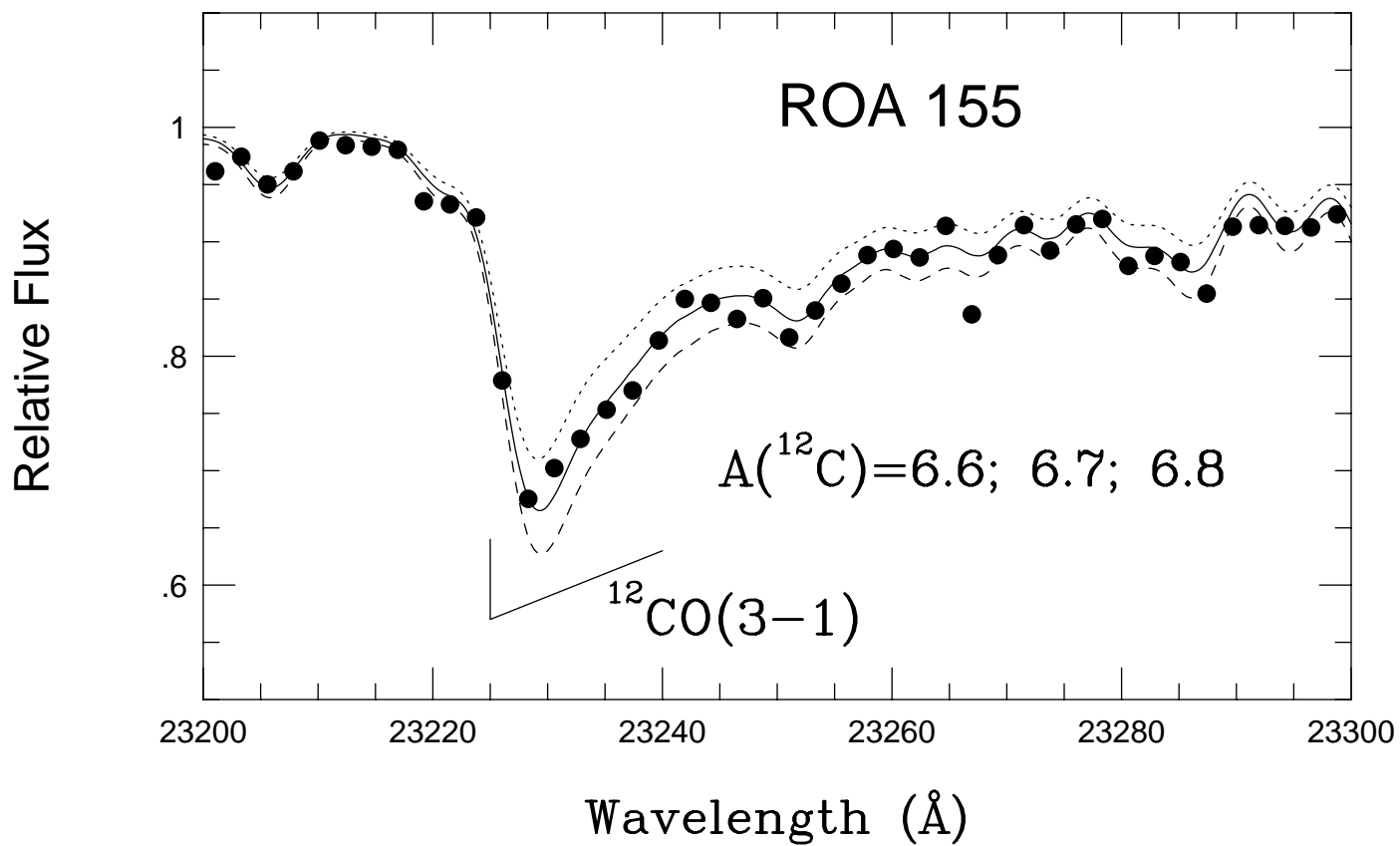


Table 3. Program Star Parameters & Isotopic Carbon Abundances

Star (ROA)	T <sub>eff</sub> (K)	Log g (cm s <sup>-2</sup> )	ξ (km s <sup>-1</sup> )	A( <sup>12</sup> C) <sup>a</sup>	[ <sup>12</sup> C/Fe] <sup>b</sup>	<sup>12</sup> C/ <sup>13</sup> C
58	4200	0.6	2.2	5.90	-0.96	7.0
91	4300	1.0	2.0	6.40	-0.46	3.5
139	4200	0.8	2.0	6.00	-1.13	3.5
150	3950	0.6	2.2	6.40	-0.94	4.0
155	4200	0.8	2.0	6.70	-0.25	4.5
161	4250	0.8	2.1	6.50	-0.42	3.5
162	3950	0.7	2.1	6.60	-0.89	3.0
252	4400	1.1	2.0	6.20	-0.65	6.0
253	4300	1.0	1.9	6.50	-0.70	3.0
287	4250	1.0	1.9	7.20	+0.04	4.0
357	4000	0.8	1.8	7.10	-0.64	5.0

<sup>a</sup>A(<sup>12</sup>C)= log  $\epsilon(^{12}\text{C})$ = log[N(<sup>12</sup>C)/N(H)] + 12.

<sup>b</sup>This ratio is computed using solar abundances of A(<sup>12</sup>C)= 8.59 and A(Fe)= 7.50, with [Fe/H] for the star taken from Norris & Da Costa (1995b)

